Site Acceptance Test Report for the ESS Raster Scanning Magnet System Pre-Series

H.D. Thomsen*, S.P. Møller
Department of Physics and Astronomy, Aarhus University (AU)
8000 Aarhus C, Denmark

May 3, 2018

Abstract

The purpose of the present document, apart from documenting the site acceptance test procedures and results, is to convey experience and considerations that could be valuable to the future system operators and engineers of interfacing hardware.

*heinetho@phys.au.dk

Contents

1 System Installation at AU

Following the Factory Acceptance Test (FAT), the system was shipped to Aarhus University (AU) and was received late in the afternoon of December 13, 2017. The shipment included all parts, except the ceramic chamber which suffered from delays from the supplier (NTG). Since the Site Acceptance Test (SAT) did not involve the chamber apart from basic verification of the ability to install and align the chamber, it was agreed to commence the testing without the chamber. About a week later, December 22, the system was ready for initial operation after:

- Support stand columns were bolted directly to the floor (apart from minor shims) and girder was lifted and placed on the $2 + 1$ support and alignment bolts of the stands. The three turnbuckles were installed and the girder was only tentatively aligned, as no testing with beam will be performed.
- Supply crates were placed in a single rack and inter-crate connections were established using the supplied cables. The supplies are powered by a single, dedicated C13 automatic circuit breaker in a 32 A ACS switchboard.
- The 4 pieces of 35 m 4-core power cables were connected to the Output Converters (OCs) and termination box. For this, only about $\simeq$ 5 m cable length would have been necessary for each of the 4 cables, and the excessive cable length was bundled into 4 respective coils. The 2×4 conductors per Raster Scanning Magnet (RSM) are connected in parallel in the termination box, *i.e.* reducing to 1 four-core cable per RSM for the short power cables [1]. The star-quad configuration is maintained as far as possible, and the cable screen is connected to the termination box grounding.
- The 2 pieces of $\simeq$ 1 m power cables, 1 per RSM were connected to the termination box and magnet coil busbars.
- Two sets of Bdot signal cables and Normally Closed (NC) loop interlock cables were routed from the termination box to the rack. The interlock signal is determined by NC thermal circuit breakers located on the magnet coils (upper and lower coil busbar connection) and matching filter panel in the termination box, all placed in series for the respective RSMs. The signals are used as input to Interlock #3 of the Control Crates (CCs), which will halt operation if the loop is opened.

1.1 Providing Pre-Triggers

To initiate a raster burst cycle, a pre-trigger signal is to be provided to the optical input ISO2 of the CC [2]: If the power supply is on and "Trig Permit" is active (indicating that the capacitor banks of CC are charged to match the current amplitude setpoint), a raster burst will be initiated by a rising edge on this input. Initially, the pre-trigger signal was generated by a simple circuit with a single HFBR-1528 optical transmitter that is driven by a signal generator to set the burst repetition rate. This simple approach could have been extended to allow a broadcast of parallel pre-triggers and thus operate the two RSMs synchronized. Instead, a stand-alone Timing EVent Receiver (EVR) system was supplied by the European Spallation Source (ESS) Integrated Control System (ICS) group [3]. This would not only allow synchronized bursting, but also enable the possibility of verifying integration of Raster Scanning Magnet System (RSMS) $\leftrightarrow$ EVR. The system was installed in the test lab on 2018.01.22 and consists of:

- Adlink-MVP-6021 with wall mountable metal plates
- PCIe-EVR-300DC (ESS TAG-402)
- IFB-300 (ESS TAG-490) + UNIV IO modules: HFBF-1414 (pre-triggers), HFBR-1528 (polarity), LEMO (TTL, pre-triggers)
- 1 ST–ST cable with two individual fibers (used for pre-triggers of RSM1 and RSM2) and 1 LC–LC for EVR loop.

The EVR system was configured for 14 Hz pre-triggers and constantly positive polarity bursts. Although testing the performance of the EVR is not within the scope of the RSMS SAT, the pre-trigger rate was tested using a scope operating in infinity persistence mode and found to steadily match the requested operation.

1.1.1 Polarity

The EVR is currently configured to provide only a constant polarity signal for the CCs, *i.e.* either constantly positive or negative burst polarity, not the intended behavior of alternating the polarity burst-by-burst. Although it has not been possible to test the alternating polarity behavior during the SAT, simple burst-by-burst polarity flips have been tested by manually configuring the EVR to do so. This at least verifies that the EVR can in fact control the burst polarity with its current configuration.

1.2 Installation of Ceramic Chamber

The ceramic chamber and test coil were installed 2018.03.14, while members of the ESS Vacuum Group were visiting to inspect the design and observe the chamber installation procedure. This involved opening both magnets:

- remove M5 pins through housing top
- retract the spring-loading mechanisms that hold the ferrite pieces in place.
- disconnect coil bus bars
- remove the magnet housing top, coil and ferrite piece while making sure that no ferrite pieces are chipped.

The procedure is now also described in further detail in the operation and service manual of the magnets [1]. A Danfysik technician conducted the operation on site while training the present AU and ESS staff members. Danfysik also provided the recommended tooling, e.g. guiding pins to remove the magnet housing top without chipping the ferrite pieces, cf. Fig. 1. AU will be removing the chamber to have it metallized at ESS. It will eventually be installed and tested again in the AU test lab to confirm that the metallization does not affect the system performance. This is expected to take place in autumn, 2018.

1.3 Coil Design

The magnet coils are vacuum resin impregnated with radiation resistant CTD101K inside a mould. The coil cross section has a large aspect ratio and a large surface area vs. its volume, thus making air convection cooling efficient. The 2D calculations from the Danfysik Detailed Design Report (DDR) [4] anticipates operating temperatures to be $\simeq$ 30–40 °C.

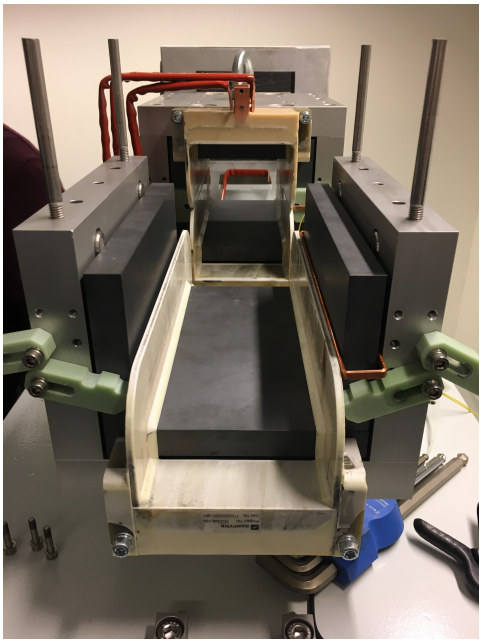

Figure 1: Installation of ceramic vacuum chamber and test coil. RSM1 having had its top, including coil and ferrite piece, removed. The four vertical pins are to guide while hoisting the top, thus minimizing the risk of chipping the top ferrite piece.

For the the pre-series coils, the resin was attempted charged with alumina powder for enhanced thermal conduction, cf. Fig. 2a. The inorganic alumina is believed to also improve the radiation hardness by an order of magnitude. This improvement is similar to when adding glass fibres to the epoxy resin matrix. It proved challenging, however, to obtain a homogeneous distribution of the alumina powder in the coils impregnation, and a number of coil impregnation designs have been produced for the main series.

Design v1: The coil is wrapped with glass tape and put into a mould. In addition, cavities (including the coil ends) are filled with glass fabrics, cf. cross sectional view in Fig. 2a. The coil is impregnated and the expected improvement in radiation hardness is about an order of magnitude. The glass fiber fill factor is $\simeq$ 50%, and the ambition was that perhaps 10% alumina could be added between the glass fibers in the epoxy matrix to improve thermal conduction. An attempt was made to add the alumina, but it was clearly rejected by the matrix.

Design v2: The mould shape was made wider, thus leaving a space on the sides of the coil where no glass was present. This void was filled with a 50% mixture of epoxy and alumina. The resulting design is as shown in Fig. 2b. The idea was that some alumina would perhaps transfer from the alumina-epoxy matrix and penetrate the outermost part of the glass reinforcement, albeit still having two relatively separate domains.

Design v3: Using the same wide mould as in the previous version, a coil insulation was cast entirely of the glass fiber matrix, cf. Fig. 2c. This design is presumed to offer the same radiation hardness as with the alumina-containing regions but perhaps slightly reduced thermal conduction properties. The latter can be assessed in the pre-series thermal testing, cf. Sec. 3.

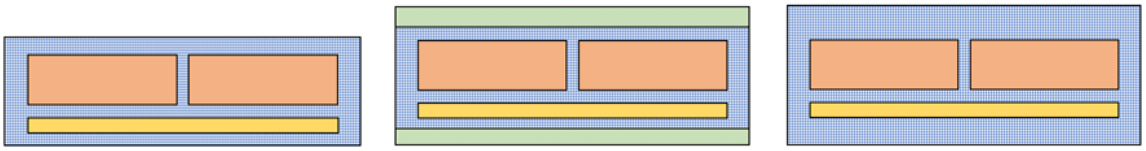

(a) Design v1: two copper conductors, a stiffening bar of G11 etronax (yellow) and a glass-reinforced epoxy matrix (blue).

(b) Design v2: an outer region of epoxy resin with 50% alumina content is added (green).

(c) Design v3: Using the same wide mould as in Design v2, a coil insulation was cast entirely of the glass fiber matrix. This design is presumed to offer the same radiation hardness as Case 2 but perhaps slightly reduced thermal conduction properties.

Figure 2: Cross sectional views of three different coil insulation solutions explored in the production of the pre-series magnets.

The RSMS was delivered with four v2 coils in the two RSMs. While the magnets were opened 2018.03.14 to install the ceramic vacuum chamber, cf. Sec. 1.2, the bottom coil of RSM1 was replaced with a v3 coil, thus enabling a direct thermal testing of the v3 design. The coil installation procedure was rather uncomplicated, apart from the new coil and its terminals being mistakenly mirrored compared to the original coils. The source of the problem was however quickly realised and a few coil busbars could be redirected to compensate for the problem. The coil chirality is introduced when bending the cut coil sheet into a saddle shape and followingly attaching the terminal connections, and the manufacturer has been made aware of the importance of this production step.

2 Monitoring System

A block diagram of the hardware that was used for the SAT can be seen in Fig. 3. Besides the RSMS equipment supplied by Danfysik and the timing system from ESS, a system was set up by AU to sample and analyse the Bdot waveforms for every burst, cf. Sec. 4.

ISAScope07 A compact 2-channel scope, PicoScope 4262 (16-bit, 10 MS/s), is used to sample the Bdot signals from the pickup loops of the RSMs. The coaxial cables are 35 m long as in the intended application at ESS. The scope features an external trigger input and the TTL signal from the EVR is used to trigger the acquisition. The scope has a USB 3.0 connection to a PC that is located in the test lab.

Local PC The Bdot data is extracted burst-by-burst using LabVIEW code. A high-priority part extracts and stores every triggered burst event in a First In, First Out (FIFO) structure [5], while a low-priority part performs data reduction and burst quality assessment. The code also logs error messages and state of the supplies through the facility control system.

ConSys The control system used throughout the AU accelerator center. The supplies are implemented as devices and the RSMS can be configured and monitored using a ConSys console. Although it was never implemented, it would have been possible to control the EVR parameters through EPICS channel access.

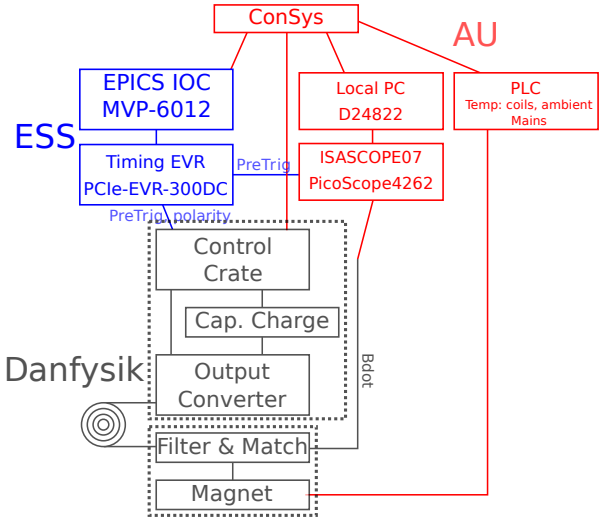

Figure 3: Block diagram of the setup in the test lab.

PLC A generic PLC is used to continuously monitor system parameters, *e.g.* the mains input electric power, temperatures of RSMS components and ambient temperatures.

3 Thermal Studies

Local temperatures can be measured using PT1000 sensors + PLC in combination with a thermal imaging camera, FLIR C2. A thermal image of the setup can be seen in Fig. 4. In this example, only RSM2 was operated and its components—the left magnet and right power cable coil—are notably warmer, albeit quite tolerable, $\lesssim$ 30 °C. As expected, the warmest components are the magnet coils, power cables, and in particular the aluminum backplate of the termination box, as will be discussed in detail later. The thermal imaging was used to locate the warmest components and strategically place the PT1000 sensors.

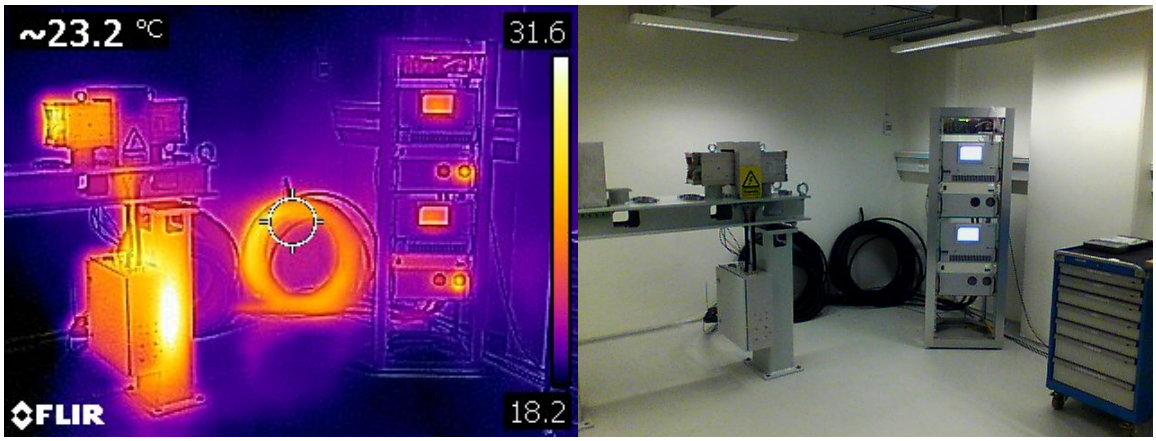

Figure 4: Thermal imaging of the system while only one RSM is operated.

Region	Sensor name	Location
Girder	pt_D3p1	RSM1, bottom coil
	pt_D3p2	RSM1, top coil
	pt_D3p3	RSM2, bottom coil
	pt_D3p4	Termination box
Rack	pt_D4p1	RSM1, Output Crate exhaust
	pt_D4p2	RSM2, Output Crate exhaust
	pt_D4p3	RSM1, power cable core
	pt_D4p4	Ambient temperature

Table 1: Location of the eight PT1000 sensors in the test lab.

Eight sensors are placed in groups of four, cf. Tab. 1. In Fig. 5 selected PT1000 readouts are presented for a $\simeq$ 2-week period while the RSMS was operated at 230 A at 40 kHz. Some fluctuation structures are visible in all time series simultaneously—*e.g.* during April 6—and are thus believed to be a display of test lab ambient temperature regulation events, not the RSMS. Besides this, the steady state temperatures can be examined and are fairly consistent with the values predicted in [6, 4].

3.1 Termination Box

The matching filter consists of two panels (one panel per RSM) of capacitors and resistors that are mounted directly on the aluminum backplate of the termination box. At full specification, 300 W is expected to be deposited in the termination box, in particular in the matching filter resistors. These require a good thermal contact with the backplate to dissipate the heat. The temperature at the back of the termination box (pt_D3p4) is at 47.7 °C after several days of operating both systems at 14 Hz, 230 A, 40 kHz. All other temperatures, *e.g.* coils and cables, are $\simeq$ 30 °C. The resistors are measured to be about 50 °C using thermal imaging, cf. Fig. 6. Preceding this picture, a single resistor was found to be considerably hotter, $\simeq$ 90 °C, cf. Fig. 7, due to inadequate amounts of thermal paste. The matching filter components are protected from excessive operational temperatures by NC thermal breakers with a breaking threshold of 65 °C. For each magnet + supply, the breaker is in series with the two thermal breakers located at the magnet coil terminals, as previously described.

3.1.1 Termination Box Cooling Solutions

Several ways of cooling the termination box have been considered for the pre-series.

Initial design. In the detailed design of the system, the matching filter heat load would be dissipated through its thermal contact with the support stand column and passive convection. During the FAT this was however found to be inadequate.

Fan + heatsink. As an intermediate solution to avoid postponing the delivery of the pre-series, a fan-based solution was implemented, while it was agreed that the main series will feature a water-cooled termination box backplate.

Fans in door. During the full RSMS assembly in Aarhus, having a large heatsink and fans mounted on the termination box was found to be in mechanical conflict with the

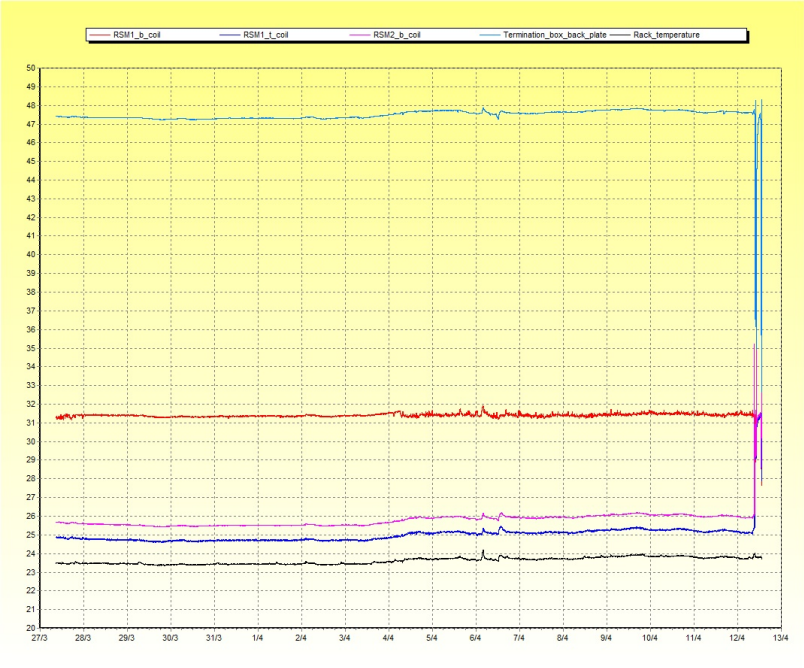

Figure 5: Visualisation of temperature measurement data from selected PT1000 sensors over the course of about 2 weeks at 230 A. The termination box backplate (light blue) is significantly warmer than the RSM1 bottom coil (red) and the ambient temperature (black). The behaviour on April 12 should be disregarded as it relates to testing at higher currents. Similarly, the sensors for RSM1 top coil (blue) and RSM2 bottom coil (pink) were not mounted during this period.

rigid short power cables connected to the magnet busbars. As a first attempt, the system was operated without any active convection, as the system was originally intended. Only limited current amplitudes of 150 A–200 A could be attained, however, without leading to interlocks due to excessive matching filter temperatures.

As a simple improvement, cooling fans were mounted in the cabinet door and exhaust holes were introduced in the cabinet. The fans would blow air directly on the panel of electrical components and the aluminum-backplate was in direct contact with the stand with thermal paste applied at the interface. Although some of the heat is successfully dissipated, the heat load at full 340 A amplitude on both lines (estimated to 300 W) is found to be excessive and would trip the thermal breakers at about 250 A. Unless else is specified, the SAT tests steps were all conducted with this cooling solution that allowed operation at 230 A.

Water-cooling tests. Danfysik performed their FAT test steps at full current amplitude using a crude water-cooling solution. Their equipment was borrowed to perform SAT studies at the maximum peak current of 340 A. Since this also involved running hoses across hallways to a water-cooling connection a few labs away, testing with water-cooling could only be justified for a few days.

Figure 8 and 9 shows thermal imaging of the full setup and a closeup of a RSM, respectively, when operating at 340 A with water-cooling. By comparing the former with Fig. 4, it is evident that the simple water-cooling circuit very efficiently cools the termination box. This is also seen in the PT1000 measurements seen in Fig. 10 where the termination box

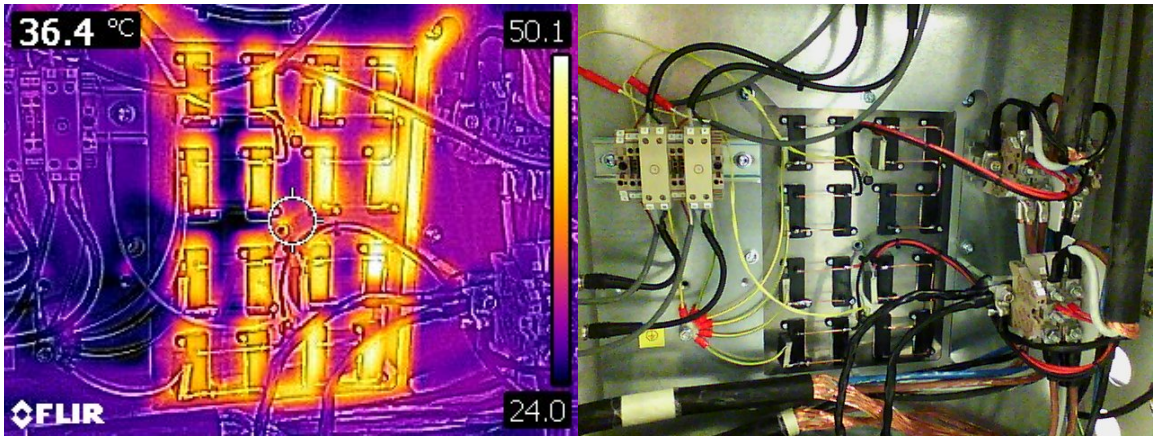

Figure 6: Thermal imaging of the inside of a termination filter. The upper and lower half of the black resistors are part of the matching filter for RSM1 and RSM2, respectively.

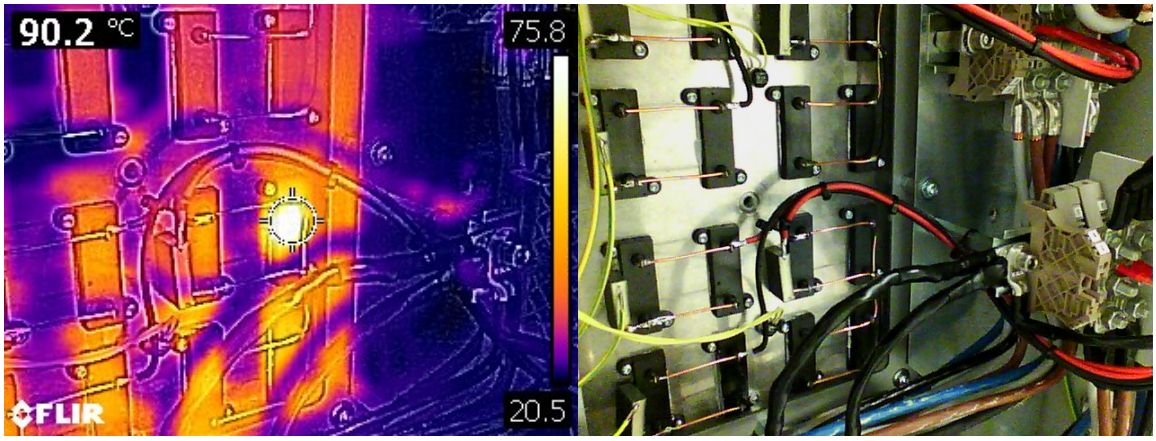

Figure 7: Thermal imaging of the inside of a termination filter: one resistor is seen to have a notably higher temperature due to poor thermal contact.

temperature is now $\simeq$ 6 °C lower than the coil temperatures. It is also seen here that it takes several hours of operation at full current amplitude for the coils to reach their steady state temperature. Since the Bdot loops are located in the vicinity of the coils, the Bdot response may also change slightly during the warm-up.

Although the cooling solution of the termination box is found inadequate in the pre-series, it should be kept in mind that the nominal operational current amplitude is $\lesssim$ 170 A at a beam energy of 2.0 GeV. With the current cooling solution we have thus been able to probe the system's long-term performance at more than 35% beyond amplitude at the ESS nominal application of the RSMS. The significant current amplitude contingency of +100% beyond nominal operation of the system is reserved for operating the system in a degraded mode, where nominal overall system performance can be provided, despite 1–2 RSMs per raster direction (horizontal or vertical) are inoperable due to local faults.

For the main series, a well-dimensioned water-cooling loop will be designed to enable operation even up to full system amplitude of 340 A.

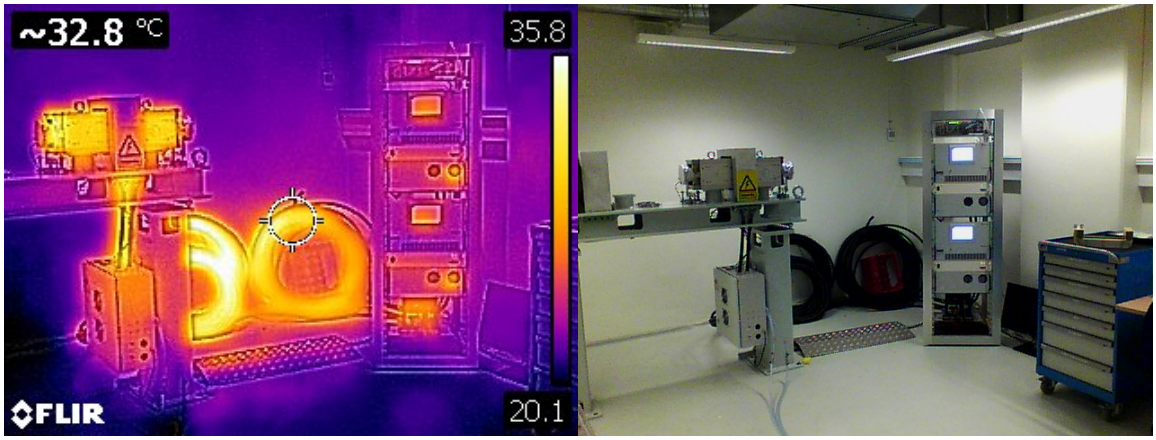

Figure 8: Thermal imaging of the setup while operating at 340 A at 40 kHz.

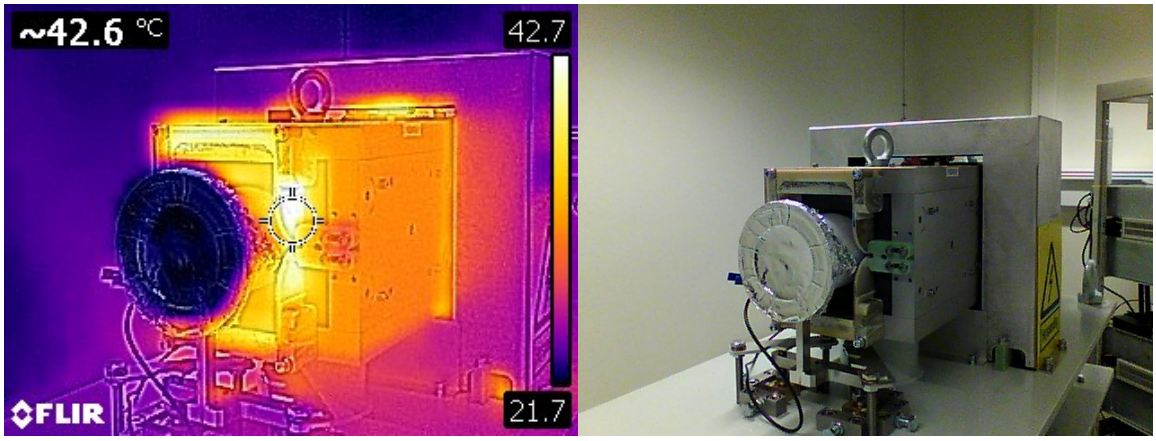

Figure 9: Thermal imaging of a RSM while operating at maximum specifications.

3.2 Coil Design Thermal Testing

Initial thermal testing of a coil without the addition of alumina was carried out at Danfysik by powering it with 90 A DC current, which is the power equivalent of operation at 14 Hz, 40 kHz, 4.2 ms burst length, and 340 A current amplitude, *i.e.* the maximum capability of the system. The DC current test led to a steady state temperature of 37 °C (and 43 °C at double the input power), which is reasonable for a passively cooled coil. For these tests the coil was not mounted in a RSM, which may affect heat convection and conduction. This is more correctly tested in the AU test lab.

Following the installation of the test coil in RSM1, this magnet has a v2 top coil (including alumina) and v3 bottom coil. After 12 hours of operation at 14 Hz, 230 A, 40 kHz the test coil temperatures are 31.5 °C (PT1000-measurement at coil ends). This is to be compared with a measurement of 31.3 °C on the top coil of the same magnet. Fig. 11 supports these numbers, where it is difficult to see a difference in the thermal performance. This is also the case at the highest current amplitudes, cf. Fig. 10. From the system owner's viewpoint, the simpler coil design would also result in less costly spare coils that could be produced by a larger selection of suppliers. Conclusively, it is suggested to change the coil design to include the simpler impregnation, not featuring alumina.

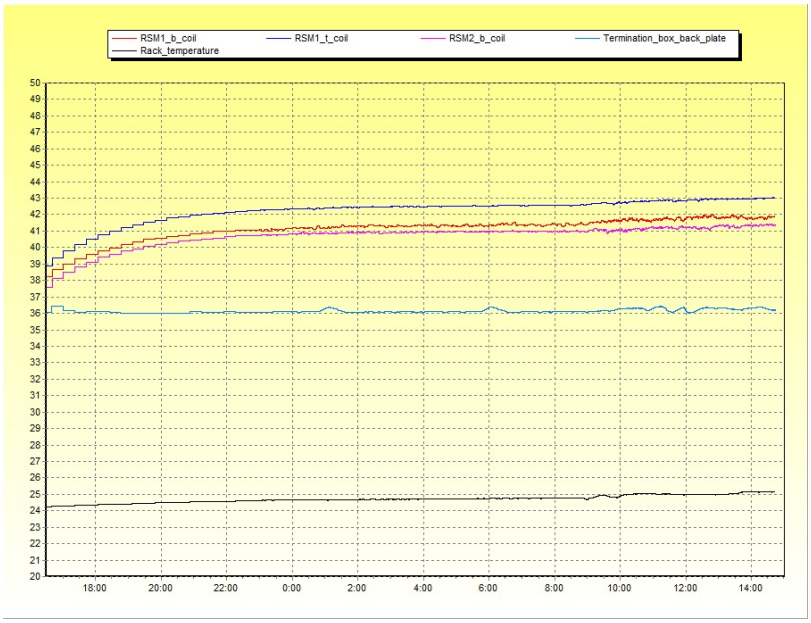

Figure 10: Visualisation of temperature measurement data from selected PT1000 sensors when operating at 340 A. The data labels are as explained in Fig. 5.

4 Characterizing the Bdot Signal

An example of the Bdot waveforms as sampled by a Tektronix scope can be seen in Fig. 12. The Bdot signals from RSM1 and RSM2 at 40 kHz operation are shown in yellow and cyan, respectively, while the TTL trigger signal is shown in green. The upper panel displays the full sample waveform—a few raster cycles of a burst in this case—while the main panel displays a zoomed region of this. The waveform shape is characterized by being rectangular with sharp edges and noticeable spikes or peaks at the switching points. The plateau level has a slight droop, but the waveform—representing the raster displacement velocity across *e.g.* the target—never falls to a significantly lower value before switching the direction. The waveform edge rise times are short, cf. FFT analysis of current waveform in [7].

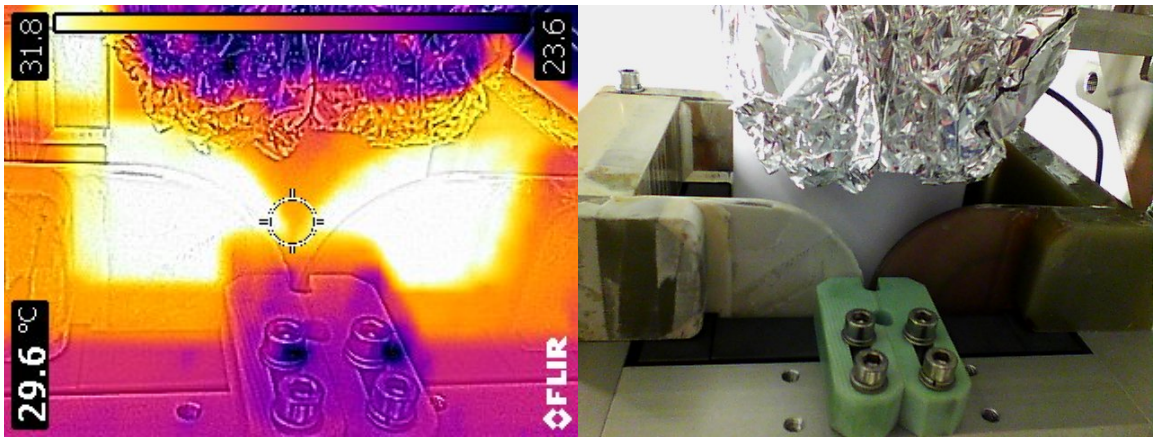

Figure 11: Thermal imaging of RSM1 coil ends: v2 coil (top) and v3 coil (bottom) are left and right, respectively, in this picture.

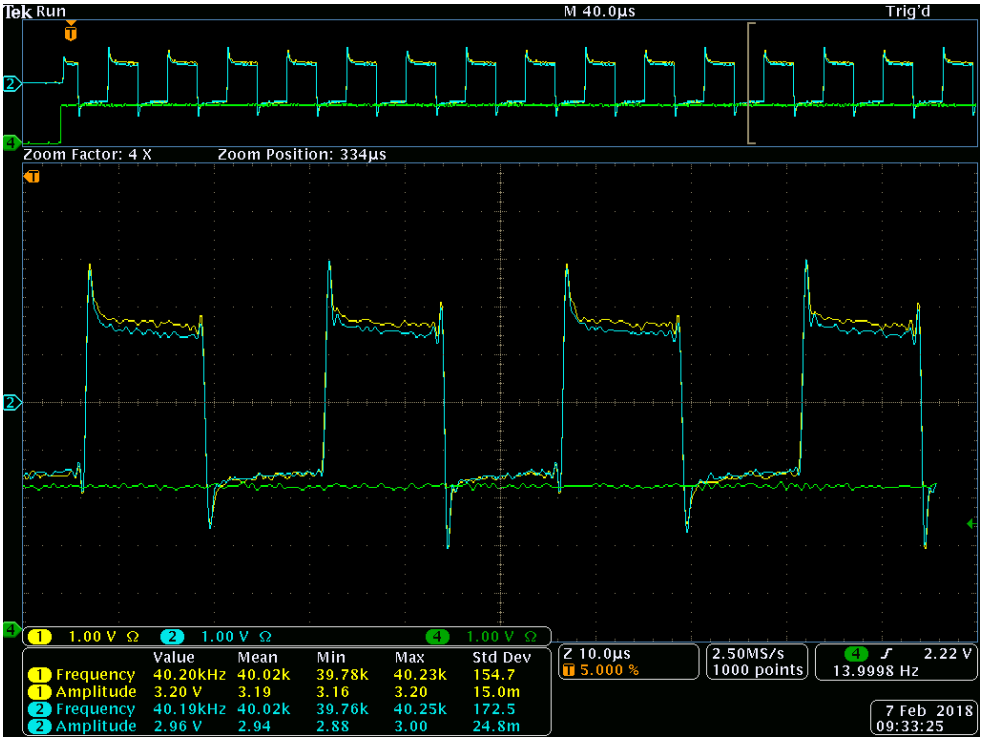

Figure 12: Scope dumps of Bdot signals from RSM1 and RSM2.

The shape is, including the overshoot after switching, strikingly similar to the predictions based on SPICE simulations [6, 4].

4.1 Calibration

A calibration of the Bdot signal amplitude vs. supply current and frequency setpoints was performed. It should be emphasized that since the Bdot signal represents the time derivative of the current waveform, the Bdot signal amplitude is ideally expected to be directly proportional to the current amplitude setpoint and inversely proportional to the raster frequency. A normalized Bdot amplitude—the detected Bdot amplitude / detected frequency—is thus devised to reconstruct the current amplitude. The motivation for the calibration was to verify the relationship described but also to examine the stability of the signal and its potential application to reconstruct (*i.e.* indirectly measure) the current amplitude. The two supplies were operated in parallel with identical parameter setpoints. The amplitude and frequency of the Bdot waveforms were determined using LabVIEW built-in waveform functions, and a 1000-point moving average and RMS of the resulting normalized Bdot signal values were used to represent the response. The results are seen in Fig. 13. The statistical errors on the datapoints are very small with relative values of the order of 10^{-4}, hardly visible on this scale. The results of a frequency variation is also partly visible in this plot as a vertical distribution of data points at the choice of constant current amplitude, 230 A. The frequency was varied between 10 kHz–40 kHz, and the normalized Bdot level was seen to be almost unaffected, as expected. By comparing the found regression coefficients, specifically $p1/p2$, the normalized Bdot response is observed to be a predominantly linear function of the current setpoint.

The normalized Bdot level is thus considered to be a stable and robust linear figure of merit for the current waveform amplitude.

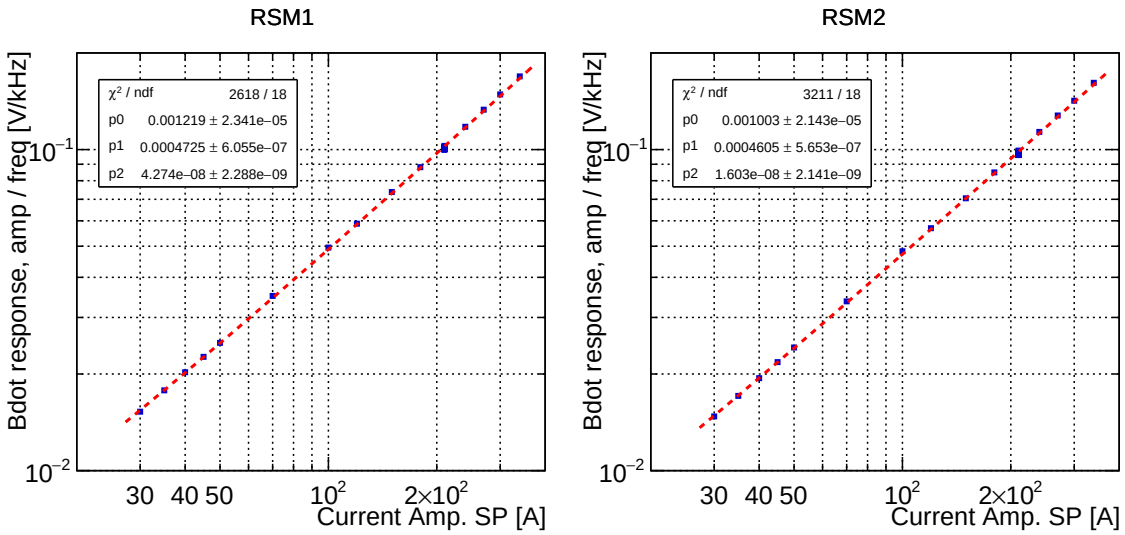

Figure 13: Calibration of the normalized Bdot signals. Left and right panels represent data from RSM1 and RSM2, respectively. The coefficients of a quadratic regression (dashed, red line) are shown as p_0–p_2 for each data set.

4.2 Crosstalk

The pre-series feature two RSMs sharing the same orientation, a RSM pair, that are placed with a magnet-to-magnet centre distance of 360 mm, leaving only 130 mm between the ferrite yokes, *i.e.* a distance comparable to the magnet gap. Some crosstalk between the Bdot signals of the adjacent magnets is thus to be expected. The effect was probed by operating one magnet, typically at 40 kHz, 14 Hz, while leaving the other magnet unpowered and vice versa. The normalized Bdot signals were measured from both magnets while increasing the current amplitude setpoint of the powered magnet. Under such circumstances, crosstalk effects were indeed detected, cf. Fig. 14. Here, RSM1 is powered (channel 1, yellow) while crosstalk is distinctly seen in the RSM2 Bdot loop (channel 2, cyan). The crosstalk has a polarity opposite of the primary signal and has considerable ringing following the switching point. Using a lower raster frequency, *e.g.* 10 kHz, cf. Fig. 14b, the settling time is observed to be about $\simeq$ 10 μs. An attempt was made to minimize the crosstalk by not routing the coaxial Bdot cables along the power cables. It would appear that the spikes near the switching points were reduced somewhat by this but the crosstalk persisted[1]. The ratio was measured for several combinations of primary current amplitude setpoint and raster frequency for both RSMs. The data is presented in Fig. 15 with errorbars indicating statistical errors only. The general amplitude level of the crosstalk signal is seen to be about 1:52 of the primary signal. Although correlations are visible, it should be kept in mind that the magnitude differences are minute in general, as the crosstalk effects are a factor $\simeq$ 52 smaller and can thus be considered a secondary effect.

Under nominal system applications, a RSM pair like the one examined here would be operating in parallel, *i.e.* sharing frequency, amplitude, polarity, and synchronization, and the crosstalk should thus not significantly distort the Bdot waveforms of the pair, apart from perhaps changing the plateau or overshoot peak amplitude to a slight degree that can

[1]The two cable types were already separated while generating the snapshots shown in Fig. 14.

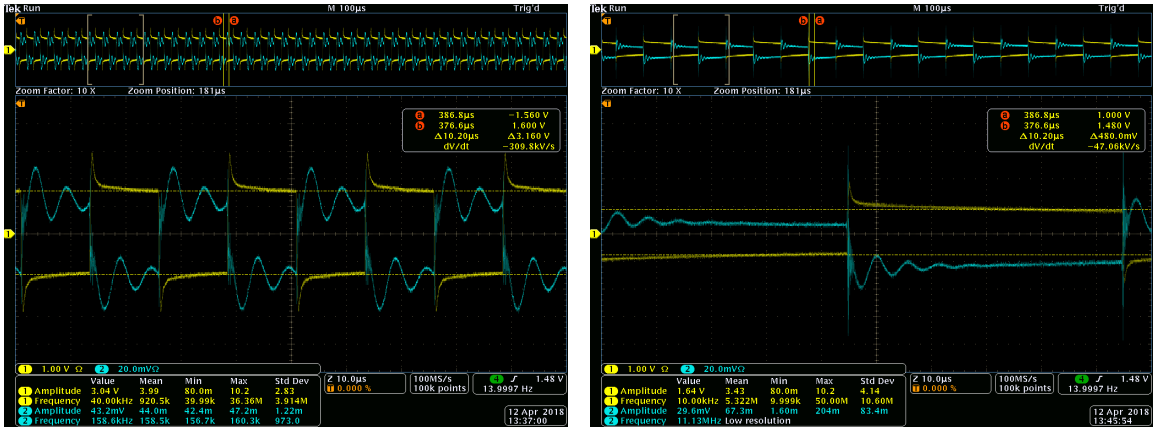

(a) Operation at 40 kHz. **(b)** Operation at 10 kHz.

Figure 14: Bdot crosstalk examples: please notice the $\times 50$ factor in vertical scales of the two channels.

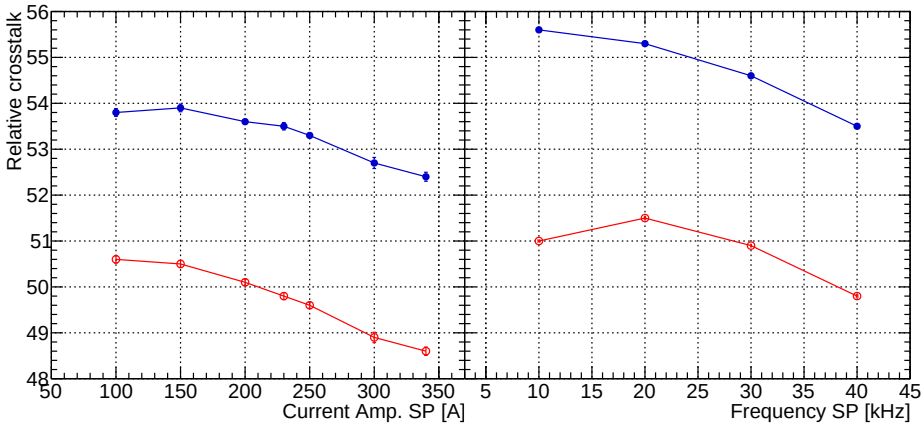

Figure 15: Bdot crosstalk measurements as a function of current amplitude setpoint (left panel) and frequency setpoint (right panel). Data from powering RSM1 and RSM2 are shown in blue and red, respectively.

be considered almost independent of frequency and current amplitude. In the full setup of the production series, the two adjacent RSMs with orthogonal magnetic field orientation will have a yoke-to-yoke distance of 360 mm, considerably longer than the 130 mm found in a RSM pair. It has not been possible to test crosstalk between two magnets in this orientation during the SAT, but the larger magnet separation combined with the measurements of stray field during the FAT argues that such effects would be negligible. Since the two pairs on a girder are expected to operate at distinct frequencies, crosstalk between pairs would yield an apparent frequency contamination in the Bdot signals, albeit only expected at levels far below 1%.

It is concluded that crosstalk effects in the Bdot signals do not influence their applicability, providing a direct indicator of the magnetic field waveforms delivered.

4.3 Data Reduction & Validation

Aiming for long-term system test periods of the order of $\simeq$ 1 month, a Bdot data reduction scheme was designed to avoid allocating an unreasonably sized data storage and eventually conducting a data analysis of a magnitude that was uncalled for. Instead, a few figures of merit are calculated for each burst. As far as possible, the chosen parameters can be used to also verify key system parameter stability requirements. As mentioned in Sec. 2, every single burst is measured and put in a FIFO structure for analysis. Waveform parameters such as amplitude, frequency, phase, *etc.* are determined using LabVIEW built-in functions. The following information is extracted from the Bdot signals for each burst:

Reconstructed peak current: using the calibration of the normalized Bdot level in Fig. 13 inversely, the measured normalized Bdot level is converted to a value for the apparent peak current of the burst.

Raster frequency: the LabVIEW function is able to determine the frequency quite accurately, with an error of better than 5 Hz at 40.000 kHz. The found value is used to normalize the Bdot levels.

Burst DC offset: the relative Bdot signal DC offset along a burst is calculated. It should however be kept in mind that the Bdot is a time derivative and thus not sensitive to any DC magnetic field contributions.

RMS of the filtered Bdot levels: to filter out fast burst effects, including the rastering, the Bdot signal is converted to a DC signal representing the Bdot amplitude. Here, it is simpler to detect *e.g.* significant droop along a burst. The conversion consists of a software rectifier + a 5 kHz low-pass filter. Setting the cutoff frequency was a tradeoff between attenuating the fast peak and spikes near the switching while retaining the slower potential effects during a 3.5 ms burst. Using a linear fit to the filtered burst level, the droop is found to be typically $\simeq$ 0.3%/3 ms. As a more general figure of merit of the stability of the, ideally constant, signal, the RMS of the filtered signal is calculated.

Phase: the phase of the waveforms relative to the TTL pre-trigger is converted from radians to time offset in ns by using the detected raster frequency. It should be noted that the absolute phase is set by the $\simeq$ 100 MHz free-running oscillator in each supply. The value is thus arbitrary but is not expected change by more than the specified $\pm$200 ns during regular bursting.

Tolerances were set for these parameters to classify acceptable burst events. In cases where the parameter directly corresponds to an ESS requirement, the acceptance tolerance was set at least a factor $\times$2 more restrictive. The tolerances are presented in Tab. 2. During the system testing, the failed events were logged including the Bdot waveform data of a few preceding and following bursts. Additionally, supply register errors were monitored and counted. The latter could arise from interlocks (magnet and termination box overheating) or if a supply rejects a pre-trigger (meaning that the internal regulation is not within acceptable margins or >14 Hz pre-triggers are received). The efficacy of this watchdog was tested both by narrowing the parameter acceptance windows and, if possible, artificially injecting system errors.

Parameter	Acceptance centroid	Acceptance tolerance	Requirement
Peak current	Setpoint	$\pm 0.5\%$	$\pm 1\%$
Frequency	Setpoint	$\pm 10^{-4}$	± 50 Hz
DC offset	0	$\pm 1\%$	—
RMS of DC level	1.6×10^{-3}	$\pm 100\%$	—
Phase	Arbitrary	± 100 ns	± 200 ns (± 1 ms)

Table 2: Parameters and the tolerances used to classify acceptable burst events during testing.

5 The RSMS Long-Term Testing

It is considered notoriously difficult to accurately predict the system reliability and availability of one-off designs and actual testing is typically relevant. The novel parameter combination of the RSMS and the considerable impact of potential failures entailed a system pre-series production step, and the pre-series is an obvious occasion to assess system availability on actual hardware. The RSMS cannot be operated to enable accelerated life testing, so a considerable amount of operational hours—comparable to the ESS production run durations—would have to be dedicated to this.

During the FAT at Danfysik, the RSMS were subjected to stability tests for only a practicable duration, *i.e.* 4–8 hours. For the SAT, a goal of 1000 hours of operation was set. The system errors are expected to be randomly occurring with causes being due to internal timing or communication error, wear-out, *etc.* It was thus argued that the pre-series Long-Term Testing (LTT) could be put on standby for short periods to make urgent tests or installations and then resume the LTT. In most of these cases, the RSMS could still be operated, while the monitoring system would suffer from downtime.

After operating the ESS RSMS pre-series system in several short test runs—of the order of 1–7 days—a dedicated LTT was initiated in the afternoon of 2018.02.16. The two raster magnets were operated in parallel by providing optical pre-triggers and polarity signals from the ESS Timing EVent Receiver (EVR) that is deployed in the test lab. The pre-triggers were broadcast at 14.0 Hz while the polarity signals were constant (positive). The Bdot signal sampling, data reduction and validation were performed by LabVIEW code for every single burst event.

The RSMS LTT was concluded $\simeq$ 8 weeks later, 2018.04.11, where the RSM system had been monitored for a period of 1188 accumulated hours, corresponding to 59.9 Mburst. While the data acquisition system has suffered from bugs that have caused monitoring downtime—during which we technically cannot vouch for the RSMS performance—the RSMS has been operational for almost 100.0% of the total run duration, seemingly also during the monitoring system downtime. The accumulated times are shown in Fig. 16. Although difficult to quantify from the figure, the RSMS was only non-operational for less than 7 hours of the test period, all of it during the ceramic chamber and coil installation, cf. Sec. 1.2.

The operational durations between interrupting the monitoring and RSMS is projected into the histograms in Fig. 17a and Fig. 17b, respectively. It may be worth emphasising that the the monitoring system and RSMS have a mean time between interruptions of 407.9 hours and 645.7 hours, respectively. Although interruptions have been introduced, the mean times between interruptions are thus considerable.

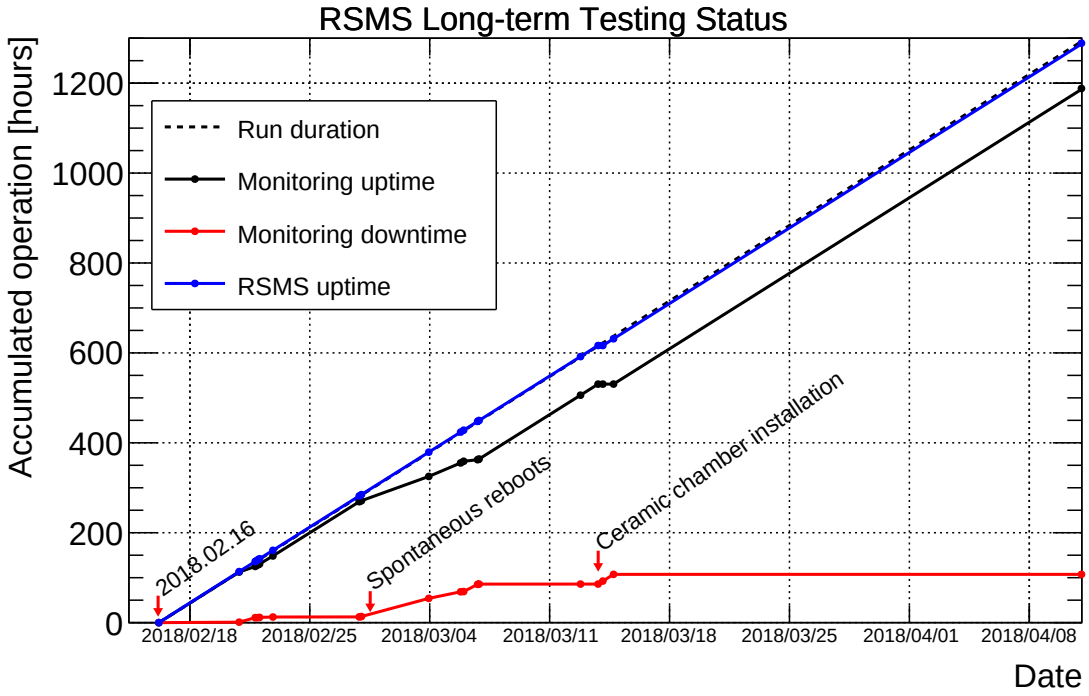

Figure 16: A plot of the accumulated times relevant to the LTT.

5.1 System Error Candidate Events

Over the course of the LTT, only three RSMS error candidates were detected and are described here.

2018.03.20. 12:05 The RMS of the filtered RSM1 Bdot levels fell outside the initial acceptance tolerance of $\pm 50\%$. Inspecting the apparently flawed burst event, no visible artefacts were present. Since this parameter's threshold is somewhat empirical, it was decided to simply increase the acceptance threshold to $\pm 100\%$ and continue.

2018.04.03. 9:27 The reconstructed current amplitude of RSM1 dropped 0.72% below the expected value—*i.e.* outside $\pm 0.5\%$— and the burst was classified as unaccepted. This outlier event is still within the ESS requirements of $\pm 1.0\%$. For a brief period, testing continued with this value set as the acceptance tolerance, but it was soon reduced to the original value, as the incident appeared to be a rogue event. The monitoring setup was analysed for flaws, and it was found that the detected Bdot amplitude could be altered $\lesssim 1\%$ by jiggling the Bdot coaxial cable close to the PicoScope BNC connector. The cables were secured to reduce the risk of accidental movement during system monitoring.

2018.04.06. 9:24 An event very similar to the one above; the reconstructed current amplitude of RSM1 dropped 0.99% below the expected value. A coincidence between the current amplitude events was that they both occurred while logging into the PC running the LabVIEW code. Although this did not appear burdened, it may have affected the monitoring process somehow.

In all cases of error candidate events it is thus difficult to ascertain the true cause of the apparent error. Additionally, we cannot discern whether the error truly relates to the RSMS

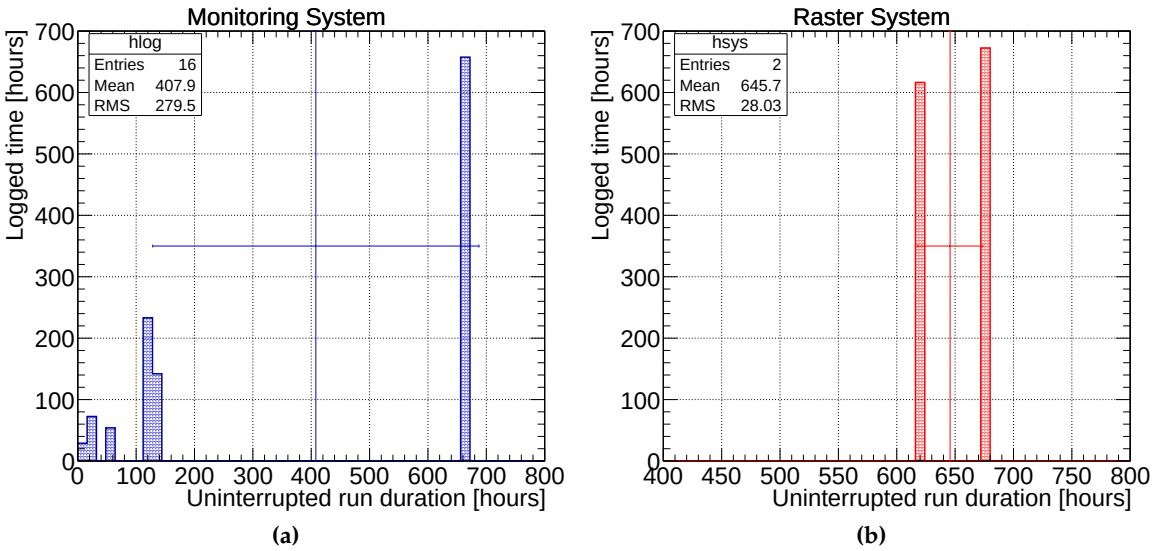

Figure 17: Distributions of uninterrupted system operation duration during the RSMS LTT. Please notice the different in horizontal scales. The vertical line is a graphical representation of the mean time between system interruption, while horizontal error bars indicate the corresponding RMS value.

or the local monitoring system. Nevertheless, only very few error candidate events have been detected throughout the Long-Term Testing (LTT), and only scheduled RSMS downtime has occurred.

6 Conclusion

Besides any potential RSMS supply error states, the Bdot signal has been utilized to test the system to the level of better than the its performance requirements. It may be that the applied monitoring hardware and the Bdot signal integrity are close to the limits of achieving this. For future—and more critical—applications of the Bdot signal, more detailed studies of the Bdot signal integrity and the application of dedicated real-time hardware should be considered, depending on the magnitude of relative errors that is to be guarded against. It may for instance be sufficient to accept current amplitudes within $\pm 10\%$, which would put lower demands on the monitoring system's accuracy and precision.

Throughout the SAT, a spreadsheet containing several design change requests has been compiled and distributed among ESS interfacing groups. Several comments and change requests have already been captured in this process. As of now, most change requests have been iterated and settled by agreement between all three parties, ESS, AU, and Danfysik.

7 Acronyms

AU Aarhus University

CC Control Crate

DDR Detailed Design Report

ESS European Spallation Source

EVR Timing EVent Receiver

FAT Factory Acceptance Test

FIFO First In, First Out

ICS Integrated Control System

LTT Long-Term Testing

NC Normally Closed

OC Output Converter

RSM Raster Scanning Magnet

RSMS Raster Scanning Magnet System

SAT Site Acceptance Test

References

[1] Danfysik, H. D. Thomsen, and S. P. Møller, "Operation and service manual. ESS Scanner Magnets on Girder," tech. rep., ESS, 2018.

[2] Danfysik, H. D. Thomsen, and S. P. Møller, "Interface Specification. Magnet Power Supply," tech. rep., ESS, 2017.

[3] J. C. Garcia and J. H. Lee, "Timing System Introduction for Raster Magnet System," tech. rep., ESS, 2018.

[4] Danfysik, H. D. Thomsen, and S. P. Møller, "Detailed design report. raster scanning magnet system for ess," tech. rep., ESS, 2016.

[5] P. Granum, "Testing of Raster Magnet for ESS," tech. rep., ESS, 2018.

[6] Danfysik, H. D. Thomsen, and S. P. Møller, "Conceptual design of raster scanning system," tech. rep., ESS, 2014.

[7] Danfysik, H. D. Thomsen, and S. P. Møller, "Factory Acceptance. Test Procedure For ESS RSMS-PS Serial No. 1700703 and 1700704," tech. rep., ESS, 2017.